

The Projected Gross-Pitaevskii Equation for harmonically confined Bose gases

P. Blair Blakie¹ and Matthew J. Davis²

¹University of Otago, P.O. Box 56, Dunedin, New Zealand

²ARC Centre of Excellence for Quantum-Atom Optics, School of Physical Sciences,
University of Queensland, Brisbane, QLD 4072, Australia

(Dated: 20th October 2004.)

We extend the Projected Gross Pitaevskii equation formalism of Davis *et al.* [Phys. Rev. Lett. **87**, 160402 (2001)] to the experimentally relevant case of harmonic potentials. We outline a robust and accurate numerical scheme that can efficiently simulate this system. We apply this method to investigate the equilibrium properties of a harmonically trapped three-dimensional Bose gas at finite temperature, and consider the dependence of condensate fraction, position and momentum distributions, and density fluctuations on temperature. We apply the scheme to simulate an evaporative cooling process in which the preferential removal of high energy particles leads to the growth of a Bose-Einstein condensate. We show that a condensate fraction can be inferred during the dynamics even in this non-equilibrium situation.

PACS numbers: 03.75.-b, 03.75.Hh

I. INTRODUCTION

The near zero temperature formalism for Bose-Einstein condensates is based upon the well-established Gross-Pitaevskii equation (GPE) that describes the macroscopically occupied condensate orbital. It has been proposed that the GPE can also be used to model the non-equilibrium dynamics of finite temperature Bose gases [1, 2, 3, 4]. The essential idea is that highly occupied modes of a quantum field are well described by a classical field, as is well-known for the case of electromagnetic fields. Recently, calculations have been performed by several groups using classical fields [5, 6, 7, 8, 9, 10, 11, 12] and have shown the usefulness of this approach. One of the key advantages of the classical field method is that it is non-perturbative; however care must be taken to appropriately cutoff the spectrum to avoid an ultraviolet catastrophe, analogous to that occurring in the Rayleigh-Jeans theory of blackbody radiation. Ideally this cutoff can be made from *a priori* thermodynamic analysis of the system. In the finite temperature formalism of Davis *et al.* [6, 7, 13], the cutoff is explicitly incorporated through the use of a projector that is diagonal in the single particle basis of the system Hamiltonian. This ensures that a consistent energy cutoff is established, and provides a natural separation of the system into regions of low energy modes (the highly occupied *coherent region*) and high energy modes (the sparsely occupied *incoherent region*). Ignoring the incoherent region and its coupling to the coherent region, the equation of motion for the low energy modes is termed the Projected Gross-Pitaevskii Equation (PGPE). By itself the PGPE can only provide a partial description of the system, however it contains the modes that are most significantly modified by the effects of interactions and are difficult to include quantitatively in traditional kinetic theories. Thus the PGPE by itself can be a useful tool for providing insight into the evolution of ultra-cold Bose gases.

The Stochastic GPE formalism developed by Gardiner and coworkers [14, 15] proposes a practical scheme for coupling the coherent and incoherent regions in a manner suitable for non-equilibrium calculations. To account for the interaction with the incoherent region, this formalism introduces noise

terms into the PGPE that transfer energy and particles into and out of the coherent region.

A related technique originating in quantum optics is the phase space method known as the truncated Wigner approximation. This was first applied to ultra-cold Bose gases by Steel *et al.* [16], and further developed by Sinatra and coworkers [17, 18, 19]. A number of recent calculations using this method can be found in Refs. [20, 21, 22, 23, 24].

The main purpose of this paper is to develop the PGPE approach for the experimentally relevant case of three dimensional harmonic traps. To do this we have adapted a recent numerical scheme by Dion and Cancès [25] by introducing an explicit energy cutoff in the single particle (harmonic oscillator) basis. We use the scheme to examine the properties of trapped gases as a function of the temperature, such as condensate fraction and density fluctuations. While some of these properties were studied in Ref. [10], we believe that our numerical method is superior and our results are free from the significant uncertainties found in this paper. Finally, as a non-equilibrium application we use the PGPE to simulate the formation of a Bose-Einstein condensate in an evaporatively cooled thermal cloud.

II. FORMALISM

The theoretical formalism we numerically implement in this paper has been developed in Refs. [6, 7, 13, 15], and here we briefly summarise the main points of this formalism, adapted for application to inhomogeneous systems.

A dilute Bose gas is well-described by the second quantized Hamiltonian

$$\hat{H} = \hat{H}_{\text{sp}} + \hat{H}_{\text{I}}, \quad (1)$$

where

$$\hat{H}_{\text{sp}} = \int d\vec{x} \hat{\psi}^\dagger(\vec{x}) \left(-\frac{\hbar^2}{2m} \nabla^2 + V_{\text{trap}}(\vec{x}) \right) \hat{\psi}(\vec{x}), \quad (2)$$

$$\hat{H}_{\text{I}} = \frac{1}{2} U_0 \int d\vec{x} \hat{\psi}^\dagger(\vec{x}) \hat{\psi}^\dagger(\vec{x}) \hat{\psi}(\vec{x}) \hat{\psi}(\vec{x}), \quad (3)$$

are the single particle and interaction Hamiltonians respectively, and $\hat{\psi}(\tilde{\mathbf{x}})$ is the quantum Bose field operator that annihilates a particle at position $\tilde{\mathbf{x}}$. The inclusion of an external trapping potential, assumed to be harmonic in form i.e.

$$V_{\text{trap}}(\tilde{\mathbf{x}}) = \frac{1}{2}m\omega_z^2(\lambda_x^2\tilde{x}^2 + \lambda_y^2\tilde{y}^2 + \tilde{z}^2), \quad (4)$$

is the major new feature of this paper as compared to the earlier numerical investigations made by one of us in Refs. [6, 7]. In Eq. (3) particle interactions have been approximated by a contact interaction of strength $U_0 = 4\pi\hbar^2 a/m$, where m is the atomic mass, and a is the s -wave scattering length. The harmonic trap geometry is defined by the angular oscillation frequencies along each axis, i.e. ω_x , ω_y , and ω_z . For convenience we express the x and y frequencies relative to ω_z , by introducing the relative frequency parameters $\lambda_x \equiv \omega_x/\omega_z$ and $\lambda_y \equiv \omega_y/\omega_z$.

The exact equation of motion for the field operator is given by the Heisenberg equation of motion

$$i\hbar\frac{\partial\hat{\psi}}{\partial t} = \left(-\frac{\hbar^2}{2m}\nabla^2 + V_{\text{trap}}(\tilde{\mathbf{x}})\right)\hat{\psi}(\tilde{\mathbf{x}}) + U_0\hat{\psi}^\dagger(\tilde{\mathbf{x}})\hat{\psi}(\tilde{\mathbf{x}})\hat{\psi}(\tilde{\mathbf{x}}). \quad (5)$$

For situations of experimental relevance the Hilbert space is enormously large, and directly solving Eq. (5) is not possible without further approximation. The essence of our approach is to split the field operator into two parts representing the coherent and incoherent regions. We define the projection operators

$$P\{F(\tilde{\mathbf{x}})\} = \sum_{n \in C} \varphi_n(\tilde{\mathbf{x}}) \int d^3\tilde{\mathbf{x}}' \varphi_n^*(\tilde{\mathbf{x}}') F(\tilde{\mathbf{x}}'), \quad (6)$$

$$Q\{F(\tilde{\mathbf{x}})\} = \sum_{n \notin C} \varphi_n(\tilde{\mathbf{x}}) \int d^3\tilde{\mathbf{x}}' \varphi_n^*(\tilde{\mathbf{x}}') F(\tilde{\mathbf{x}}'), \quad (7)$$

where $n \in C$ defines the modes that make up the coherent region C , and $\varphi_n(\tilde{\mathbf{x}})$ is the n th eigenfunction of the basis that diagonalizes single particle Hamiltonian \hat{H}_{sp} . We define

$$\begin{aligned} \hat{\Psi}(\tilde{\mathbf{x}}) &= P\{\hat{\psi}(\tilde{\mathbf{x}})\}, \\ \hat{\eta}(\tilde{\mathbf{x}}) &= Q\{\hat{\psi}(\tilde{\mathbf{x}})\}, \end{aligned} \quad (8)$$

which we refer to as the coherent ($\hat{\Psi}$) and incoherent ($\hat{\eta}$) field operators respectively. This division is based on the average occupation of the states. The coherent field $\hat{\Psi}$ is chosen to describe the low-lying highly occupied states of the system, i.e. modes containing of order five or more particles. The incoherent field $\hat{\eta}(\tilde{\mathbf{x}})$ contains the complementary states which are sparsely occupied. Our particular interest is in situations near equilibrium, where this separation can be conveniently introduced via thermodynamic arguments by making an appropriate energy cutoff \tilde{E}_{cut} in the single particle spectrum.

To derive the PGPE, we apply the projection operator (6) to the equation of motion for the field operator (5). The fundamental approximation we make, often referred to as the classical field approximation, is to neglect the quantum mechanical

nature of coherent field operator, i.e. set $\hat{\Psi}(\tilde{\mathbf{x}}) \rightarrow \Psi(\tilde{\mathbf{x}})$ (a c-number function) due to the high occupation numbers of these modes. By making this approximation, the equation of motion (5) is transformed to a form involving couplings between the coherent and incoherent fields of some complexity, (e.g. see [13]). As a further approximation we neglect the interaction between the coherent and incoherent regions and simply consider the equation of motion for $\Psi(\tilde{\mathbf{x}})$ in isolation

$$\begin{aligned} i\hbar\frac{\partial\Psi(\tilde{\mathbf{x}})}{\partial t} &= \left(-\frac{\hbar^2}{2m}\nabla^2 + V_{\text{trap}}(\tilde{\mathbf{x}})\right)\Psi(\tilde{\mathbf{x}}) \\ &+ P\left\{U_0|\Psi(\tilde{\mathbf{x}})|^2\Psi(\tilde{\mathbf{x}})\right\}, \end{aligned} \quad (9)$$

which is the Projected Gross-Pitaevskii equation (PGPE). This equation is of a similar form as the usual Gross-Pitaevskii equation, however the classical field $\Psi(\tilde{\mathbf{x}})$ has a distinct interpretation: It represents the quantum field for many low-lying modes, rather than just the condensate mode. Several substantial approximations have been made to reduce the full Heisenberg equation of motion for the field (5) to the PGPE (9), however previous studies have demonstrated that this final form contains a rich set of physics (e.g. see [6, 7, 9, 10]).

III. NUMERICAL APPROACH

The modes of the system are of central importance in the assumptions used to derive the PGPE, and care must be taken in numerical implementations to ensure the modes are faithfully represented. It is in our opinion that any useful simulation technique must satisfy the following requirements:

1. The space spanned by the modes of the simulation should match that of the coherent region of the physical system being simulated as closely as possible. That is, the modes should be the single particle modes of the system up to the prescribed energy cutoff \tilde{E}_{cut} .
2. The assumption of high occupancy in all modes necessitates that the numerical scheme must propagate all modes accurately.

Most commonly used methods for propagating Schrödinger-type equations do not satisfy these requirements, in particular many methods do not propagate all modes of the numerical basis faithfully. This leads to negligible errors if the highest modes are unoccupied, as is the case for the $T = 0$ GPE. However, it is clear that methods based on such assumptions will not be appropriate for simulating the PGPE.

Before introducing the numerical scheme used in this paper, we review how the method used by Davis *et al.* [6, 7, 8] to simulate homogeneous Bose gases addresses the aforementioned conditions. For the homogeneous system the modes are plane-wave like and are suitable to grid (Fourier) methods of propagation (also used in [12]). To define the coherent region Davis *et al.* instigated an energy cutoff by using an explicit projection operator in momentum space, ensuring condition 1 was satisfied. To satisfy condition 2, sufficiently many states

outside the cutoff should be retained to ensure that the nonlinear terms in the evolution equation were exactly evaluated (without aliasing) for all modes of the coherent region. This was not realized at the time and aliasing is present in the calculations presented in [6, 7, 8]. However, the presence of aliasing mainly modifies the action of the nonlinear term and does not affect the equilibrium state or the conclusions reached in these papers. For further details we refer the reader to [26].

We comment that simply using an unmodified grid method as in [12] does introduce a cutoff into the system in momentum space, but does not satisfy the two criterion listed above. First, the energy cutoff is anisotropic, varying in magnitude by a factor of three with direction in momentum space (in three dimensions). Second, the largest momentum states will be aliased in the calculation of nonlinear terms and their dynamics will be misrepresented. The situation is even worse when using an unmodified grid method to simulate classical field dynamics for a trapped Bose gas as in [5, 10, 11]. It is this issue that we address here.

A. Brief review of numerical method

The method we have used to simulate the Projected Gross-Pitaevskii equation (9) with an explicit cutoff in energy derives from a recent numerical scheme by Dion *et al.* [25]. We briefly review our adaption of this method.

To begin we rescale the Projected Gross-Pitaevskii equation (9) by introducing units of distance $x_0 = \sqrt{\hbar/2m\omega_z}$, time $t_0 = \omega_z^{-1}$, and hence energy $\hbar\omega_z$, with ω_z the trap frequency along the z -direction. With these choices, we have

$$i\frac{\partial\Psi}{\partial t} = -\nabla^2\Psi + \frac{1}{4}(\lambda_x^2 x^2 + \lambda_y^2 y^2 + z^2)\Psi + C|\Psi|^2\Psi \quad (10)$$

where we have defined the nonlinear coefficient as $C = N_C U_0 / \hbar\omega_z x_0^3$, and for clarity have used untilded variables to indicate quantities expressed in computational units. We take the wave function to be normalized to unity, so that the total number of atoms within the coherent region, N_C , appears in the definition of the nonlinearity constant. To simplify our discussion of the numerical method, we will take the harmonic trapping potential to be isotropic, i.e. $\lambda_x = \lambda_y = 1$. This allows us to avoid using cumbersome notation to account for different spectral bases in each direction.

The classical field $\Psi(\mathbf{x}, t)$ is expanded as

$$\Psi(\mathbf{x}, t) = \sum_{\{l,m,n\} \in \mathcal{C}} c_{lmn}(t) \varphi_l(x) \varphi_m(y) \varphi_n(z), \quad (11)$$

where $\{\varphi_n(x)\}$ are the eigenstates of the 1D harmonic oscillator Hamiltonian satisfying

$$\left[-\frac{d^2}{dx^2} + \frac{1}{4}x^2 \right] \varphi_n(x) = \epsilon_n \varphi_n(x), \quad (12)$$

with eigenvalue $\epsilon_n = (n + \frac{1}{2})$. The energy cutoff is implemented by restricting the summation indices to the set

$$\mathcal{C} = \{l, m, n : \epsilon_l + \epsilon_m + \epsilon_n \leq E_{\text{cut}}\}, \quad (13)$$

with the value of E_{cut} chosen to be appropriate for the physical system under consideration. For later convenience we define n_{cut} to be the largest index occurring in \mathcal{C} , i.e. the quantum number of the highest energy oscillator state in the coherent region (i.e. $n_{\text{cut}} \approx \tilde{E}_{\text{cut}}/\hbar\omega_z$).

In the basis representation, the PGPE (10) takes the form

$$\frac{\partial c_{lmn}}{\partial t} = -i[\epsilon_l + \epsilon_m + \epsilon_n + CF_{lmn}(\Psi)], \quad (14)$$

where

$$F_{lmn}(\Psi) \equiv \int d^3\mathbf{x} \varphi_l^*(x) \varphi_m^*(y) \varphi_n^*(z) |\Psi(\mathbf{x}, t)|^2 \Psi(\mathbf{x}, t), \quad (15)$$

is the matrix element of the nonlinear term. An important observation made in Ref. [25] is that these matrix elements (15) can be computed exactly with an appropriately chosen Gauss-Hermite quadrature. To show this we note that because the harmonic oscillator states are of the form $\varphi_n(x) \sim H_n(x) \exp(-x^2/4)$, where $H_n(x)$ is a Hermite polynomial of degree n , the wave function can be written as

$$\Psi(\mathbf{x}) = Q(x, y, z) e^{-(x^2+y^2+z^2)/4}, \quad (16)$$

where $Q(x, y, z)$ is a polynomial that, as a result of the cutoff, is of maximum degree n_{cut} in the independent variables.

It follows that because the interaction term (15) is fourth order in the wave function, it can be written in the form

$$F_{lmn}(\Psi) = \int d^3\mathbf{x} e^{-(x^2+y^2+z^2)} P(x, y, z), \quad (17)$$

where $P(x, y, z)$ is a polynomial of maximum degree $4n_{\text{cut}}$ in the independent variables. Identifying the exponential term as the usual weight function for Gauss-Hermite quadrature, the integral can be exactly evaluated using a three-dimensional spatial quadrature grid of $8(n_{\text{cut}})^3$ points. Thus we have verified that the matrix elements $F_{lmn}(\Psi)$ can be exactly calculated. We refer the reader to Ref. [25] for more details of how to efficiently implement the spatial transformation and numerical quadrature.

IV. SIMULATION PROCEDURE

A. Micro-canonical ergodic evolution

The evolution of the classical field preserves several constants of motion. These can be considered as macroscopic parameters that constrain the micro-states available to the system. For the PGPE, the most important such constant of motion is the total energy, given by the energy functional

$$E[\Psi] = \int d^3\tilde{\mathbf{x}} \left[\Psi^*(\tilde{\mathbf{x}}) \left(-\frac{\hbar^2}{2m} \nabla^2 + V_{\text{trap}}(\tilde{\mathbf{x}}) \right) \Psi(\tilde{\mathbf{x}}) + \frac{1}{2} U_0 |\Psi(\tilde{\mathbf{x}})|^4 \right]. \quad (18)$$

Another important constant of motion is the field normalization, given by

$$N[\Psi] = \int d^3\tilde{\mathbf{x}} |\Psi(\tilde{\mathbf{x}})|^2.$$

As discussed in section III A, we take the classical field to be normalized to unity for the initial condition: a scaling choice that causes the coefficient of the nonlinear term in the PGPE to be proportional to the initial number of particles in the coherent region. The PGPE may have other constants of motion, such as angular momentum components in traps with the appropriate symmetry, however here we will only consider situations where these are approximately zero and can be neglected.

The lowest energy solution to the energy functional is given by the time-independent Gross-Pitaevskii equation (e.g. see Ref. [27]). We denote the energy of this solution E_g . This solution corresponds to $T = 0$, however this situation lies outside the validity regime of the PGPE since only a single mode, i.e. the condensate mode, is highly occupied. For application of the PGPE our interest is in regimes with $E > E_g$ such that the system is at finite temperature with many highly occupied modes.

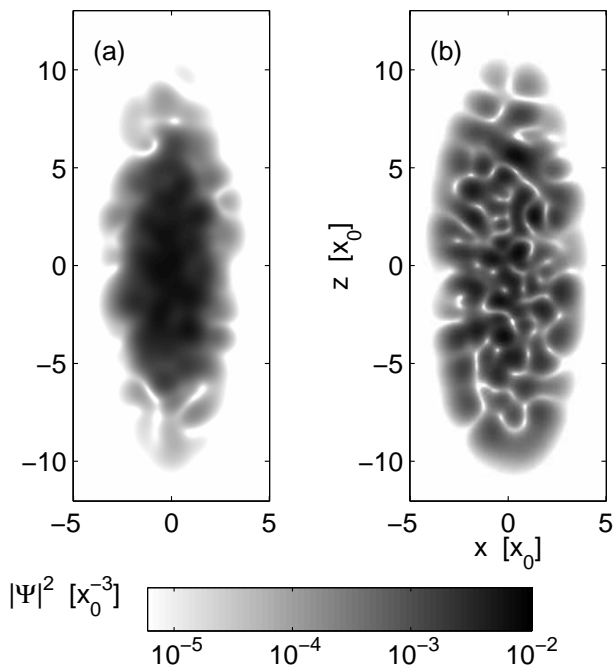


Figure 1: Thermalized classical fields for two values of energy. Density slices taken in the $y = 0$ plane for a system in an anisotropic trap with $\lambda_x = \sqrt{8}$ and $\lambda_y = 1$. (a) Low energy case with an average energy per particle of $E = 10\hbar\omega_z$. (b) Higher energy case with an average energy per particle of $E = 24\hbar\omega_z$. For both simulations $C = 2000$ and the ground state energy is $E_g = 8.54\hbar\omega_z$. The single particle cutoff energy is $E_{\text{cut}} = 31\hbar\omega_z$, below which 1739 single particle states remain in the coherent region.

For the simulations we present here we make use of the ergodic hypothesis, which we discuss further below. However, an immediate consequence of ergodicity for the study

of equilibrium properties is that the precise details of the initial conditions in a simulation are irrelevant. In practise we choose initial conditions to provide the desired values for the constants of motion. The amplitudes for each single particle mode have a random phase and occupation, but are constrained to fix the overall normalization to unity and the energy to the desired value. In general such an initial choice will not be a typical equilibrium state, but under evolution the system rapidly thermalizes. This thermalization process has been investigated for the homogeneous case in [7]. In Fig. 1 we show typical density profiles of thermalized classical fields for the harmonically trapped system. The cases in Fig. 1(a) and (b) differ in the energy of the fields. It is clear from these figures that the classical field has a somewhat chaotic appearance, and this undergoes constant evolution as the constituent modes mix through the nonlinear interaction.

B. Time-averaging correlation functions

The energy functional (18) is nonlinear, and it is not feasible to determine the entire *phase space* of classical field configurations consistent with a particular choice of energy. This prohibits the calculation of quantities using an ensemble averaging approach. However, we can determine correlation functions for the system by using the ergodic hypothesis, i.e. replacing ensemble averages by time-averages following the prescription

$$\langle F_C[\Psi(\mathbf{x})] \rangle_{\text{ensemble}} = \lim_{\theta \rightarrow \infty} \left\{ \frac{1}{\theta} \int_0^\theta d\tau F_C[\Psi(\mathbf{x}, t)] \right\},$$

where $F_C[\Psi(\mathbf{x})]$ is some functional (correlation function) of the field.

The general spatial correlation functions we are interested in are usually expressed as an ensemble average over a product of quantum field operators such as

$$F_Q = \langle \hat{\Psi}^\dagger(\mathbf{x}_1) \dots \hat{\Psi}^\dagger(\mathbf{x}_j) \hat{\Psi}(\mathbf{x}_{j+1}) \dots \hat{\Psi}(\mathbf{x}_n) \rangle.$$

Note that we have only considered correlation functions that involve the field operator for the coherent region. Also we have restricted our attention to same-time correlations, however in principle multi-time correlation functions could also be computed. To evaluate these correlation functions within the framework of the classical field theory we make the substitution $\hat{\Psi}(\mathbf{x}) \rightarrow \Psi(\mathbf{x})$, as discussed in section II, and replace ensemble averaging with time averaging. The resulting expression that we evaluate numerically is

$$\langle F_C[\Psi(\mathbf{x})] \rangle_{\text{timeave.}} = \frac{1}{N_s} \sum_{j=1}^{N_s} F_C[\Psi(\mathbf{x}, t_j)],$$

where $\{t_j\}$ is a set of N_s equally spaced time instances at which the classical field has been calculated. For this choice to well-approximate the ensemble average we require $N_s \gg 1$, and the time span over which averaging is done to be long compared to the slowest time scale in the problem, e.g. the

longest harmonic oscillator period. For the equilibrium results we present in this paper these conditions are well satisfied: we use 1400 discrete samples of the classical field taken over an evolution time of approximately 191 oscillator periods (i.e. $t_{N_s} - t_1 = 1200/\omega_z$).

C. Temperature

For comparison with experiments and other theories it is crucial to be able to identify the temperature of the classical field simulations rather than characterize a particular result by its energy. Previous attempts to determine temperature have been based on fitting the occupation of high energy modes to perturbative calculations for the spectrum based on Hartree-Fock-Bogoliubov (HFB) theory [6, 7]. For harmonically trapped gases, calculation of the HFB modes is much more difficult, and limits temperature calculations to perturbative regimes. Góral *et al.* [10] have estimated the temperature in harmonically trapped classical field simulations in a manner analogous to that done in experiments, by fitting the high momentum components of the system to a noninteracting distribution. The results of that analysis suffered from excessively large errors, and indicate this approach would not be useful for any systematic investigation of thermodynamic properties. In addition, the high energy modes of these calculations are unlikely to have been represented accurately [28].

In recent work [8] one of us has generalized Rugh's dynamical definition of temperature [29] to the PGPE. This scheme has the advantage that it is non-perturbative, and is quite accurate. This scheme can be extended to the harmonically trapped case and is used to calculate the temperature of the simulations presented in this paper. Because the implementation of this scheme in the harmonically trapped case is a trivial extension to the homogeneous implementation, we refer the reader to Ref. [8] for details.

V. RESULTS

For the results presented in this paper we have simulated a 3D system with $\lambda_x = \sqrt{8}$, $\lambda_y = 1$ and an energy cutoff of $E_{\text{cut}} = 31\hbar\omega_z$. This choice leads to a coherent region containing 1739 harmonic oscillator modes.

A. Condensation

1. Condensate fraction

Identification of the condensate fraction and mode function for an inhomogeneous system with interactions is nontrivial. This issue was addressed by Penrose and Onsager in 1956 [30], who extended the concept of Bose-Einstein condensation from an ideal gas to the case of superfluid helium. Their primary criterion for condensation is that a single eigenvalue, n_0 , of the one-body density matrix, $\rho(\mathbf{x}, \mathbf{x}')$, becomes an extensive parameter of the system. With regard to obtaining a

quantitative description of the condensate, they also showed that n_0 and its corresponding eigenvector are the condensate occupation and mode respectively.

The one-body density matrix can be written as an ensemble average of the quantum field operators as follows:

$$\rho(\mathbf{x}, \mathbf{x}') \equiv \langle \hat{\psi}^\dagger(\mathbf{x})\hat{\psi}(\mathbf{x}') \rangle_{\text{ensemble}}. \quad (19)$$

As we neglect the incoherent region in this paper, we restrict our consideration to the one-body density matrix for the coherent region, i.e. $\rho_C(\mathbf{x}, \mathbf{x}') \equiv \langle \hat{\Psi}^\dagger(\mathbf{x})\hat{\Psi}(\mathbf{x}') \rangle_{\text{ensemble}}$, and using the procedure outlined in section IV B, we calculate this matrix as

$$\rho_C(\mathbf{x}, \mathbf{x}') \approx \frac{1}{N_s} \sum_{j=1}^{N_s} \Psi^*(\mathbf{x}, t_j)\Psi(\mathbf{x}', t_j). \quad (20)$$

It is more convenient numerically to represent the density matrix in the spectral representation,

$$\rho_{ij} = \frac{1}{N_s} \sum_{n=1}^{N_s} c_i^*(t_n)c_j(t_n), \quad (21)$$

where $c_j(t_n)$ are the spectral amplitudes of the classical field at time t_n , and the index j labels all three quantum numbers needed to specify the oscillator mode that c_j refers to. The efficiency of the spectral representation affords us the ability to work with the *entire* one-body density matrix. The one-body density matrix was also time-averaged in the grid based method reported in Ref. [10], however their analysis was limited to the s -wave component.

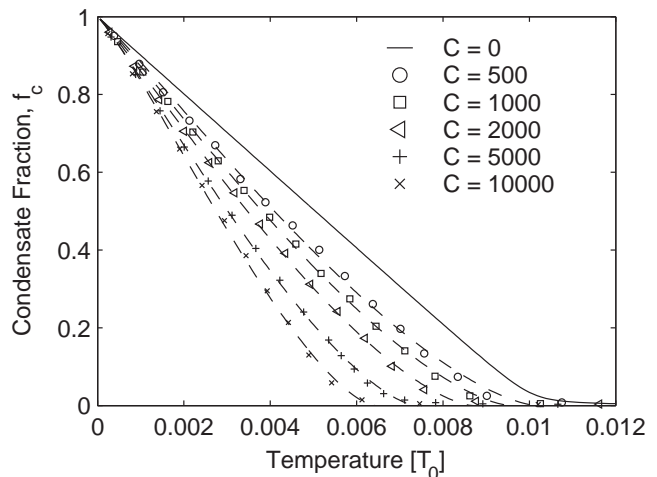


Figure 2: Equilibrium condensate occupation as a function of temperature for a range of interaction strengths. The $C = 0$ case is computed using the equipartition relation for the modes of the coherent region only. The dashed lines are simple polynomial fits to the numerical results. Other simulation parameters are the same as in Fig. 1. The averaging was performed using $N_s = 1400$ samples over a evolution period of $T = 1200/\omega_z$. The unit of temperature is $T_0 = N\hbar\omega_z/k_B$ [8], where k_B is the Boltzmann constant.

In Fig. 2 we show the condensate fraction ($f_c \equiv n_0/N_C$) as a function of system temperature for a range of interaction strengths. The rather distinctive shape of the curves arises because these calculations are for fixed N_C and E_{cut} . For a real system with a fixed total number of particles, the portion of atoms in the coherent region and the cutoff energy used to define the coherent region will change with temperature. These issues will be important considerations in making experimental comparisons, however in this paper we concern ourselves with characterizing properties of the classical field method and will only consider the case of N_C and E_{cut} as being fixed and independent of temperature.

For the interacting homogeneous Bose gas there is no mean field shift of the critical temperature. Instead critical fluctuations give the leading order shift with interaction strength to the transition temperature, and this shift is upwards. In the trapped system there is a mean field effect on the transition which reduces the critical temperature [31]. In Fig. 2 we observe this downward shift in the transition temperature as the interaction strength is increased, in qualitative agreement with recent experiments by Gerbier *et al.* [32]. We refer the reader to [33] for the application of the PGPE as a quantitative model of these experiments.

a. Suitable averaging to determine the condensate fraction: Using linear algebra arguments it can be shown that the condensate fraction determined according to the prescription we have outlined above will have a lower bound of

$$f_c \geq \max\{1/N_s, 1/G_C\}, \quad (22)$$

where N_s is the number of samples used to construct the density matrix in Eq. (21), and G_C is the number of single particle states in the coherent region. Typically we take $N_s < G_C$ so that $1/N_s$ forms a lower bound for the condensate fraction. Equality in the bound holds if the individual classical fields included in the time-average are mutually orthogonal, i.e. if $\sum_j c_j^*(t_m)c_j(t_n) = \delta_{mn} \forall \{m, n : 1 \leq m, n \leq N_s\}$. Result (22) implies, for instance, that to determine a condensate fraction below 1% will require us to take $N_s > 100$ samples.

2. Condensation: influence on density distributions in momentum and position space

It is interesting to consider how the presence of a condensate affects the position and momentum density profiles of the system. Indeed, it was the appearance of an anisotropic peak in the momentum distribution that was used as one of the signatures of condensation in the first experiments [34]. In Figs. 3(a)–(c) we compute the momentum column density for cases above and below the transition temperature. In detail, the quantity we calculate is the momentum space column density given by $\int dk_y |\Phi(\mathbf{k}, t)|^2$ (i.e. integrated along the k_y -direction), where $\Phi(\mathbf{k}, t) = (2\pi)^{-3/2} \int d^3\mathbf{x} \exp(-i\mathbf{k} \cdot \mathbf{x}) \Psi(\mathbf{x}, t)$ is the momentum space wave function and $\mathbf{k} = (k_x, k_y, k_z)$. Time-averaging this, i.e.

calculating

$$\rho_K(k_x, k_z) = \frac{1}{N_s} \sum_{j=1}^{N_s} \int dk_y |\Phi(\mathbf{k}, t_j)|^2,$$

yields the average column density shown in Figs. 3(a)–(c). The peak momentum density of the three cases considered varies over a wide range and for presentation clarity we have used a logarithmic density scale in Figs. 3(a)–(c). The appearance of a narrow peak in the momentum distribution for the condensed state is clearly observed in Figs. 3(b) and (c), however the logarithmic density scale somewhat suppresses the prominence of this feature: the peak momentum column density in Fig. 3(c) is 26 times larger than the peak density in Fig. 3(a). We also note that the momentum distribution changes from being isotropic in Fig. 3(a) where there is no condensate (as calculated according to the criterion in Sec. V A 1) to exhibiting distinctive anisotropy for the condensate momentum peak in Figs. 3(b) and (c). This anisotropy is directly related to the ratio of the trap frequencies. The usual experimental method for imaging the momentum distribution is to take an absorption image of the system after allowing it freely expand in the absence of the trap. Interaction effects during expansion significantly suppresses the contrast in momentum widths of condensed and uncondensed systems. However, the contrast has been revealed by experiments using Bragg spectroscopy techniques [35] that are able to probe the momentum distribution *in situ*.

Similarly we can construct the column density distribution in position space as

$$\rho_R(x, z) = \frac{1}{N_s} \sum_{j=1}^{N_s} \int dy |\Psi(\mathbf{x}, t_j)|^2.$$

This is equivalently obtained by integrating out the y -direction of the diagonal one-body density matrix $\rho_C(\mathbf{x}, \mathbf{x})$ (20). These distributions are shown (beneath the associated momentum distribution) in Figs. 3(d)–(f). These results emphasize that while the momentum distribution undergoes substantial changes at the transition as discussed above, the position distribution changes in a much more subtle manner. The calculations presented in [10] looked only at the behavior of slices through the position distribution of the field.

B. Density Fluctuations

Determining the condensate fraction using the Penrose-Onsager criterion is a probe of first-order coherence in the system. Indeed, the existence of a condensate is equivalent to *off-diagonal long-range order*, i.e. the system is spatially coherent. To fully characterize the field it is necessary to consider higher-order correlations in the system.

To demonstrate the usefulness of the PGPE, we use it to calculate the normalized n -th order coherence function at zero

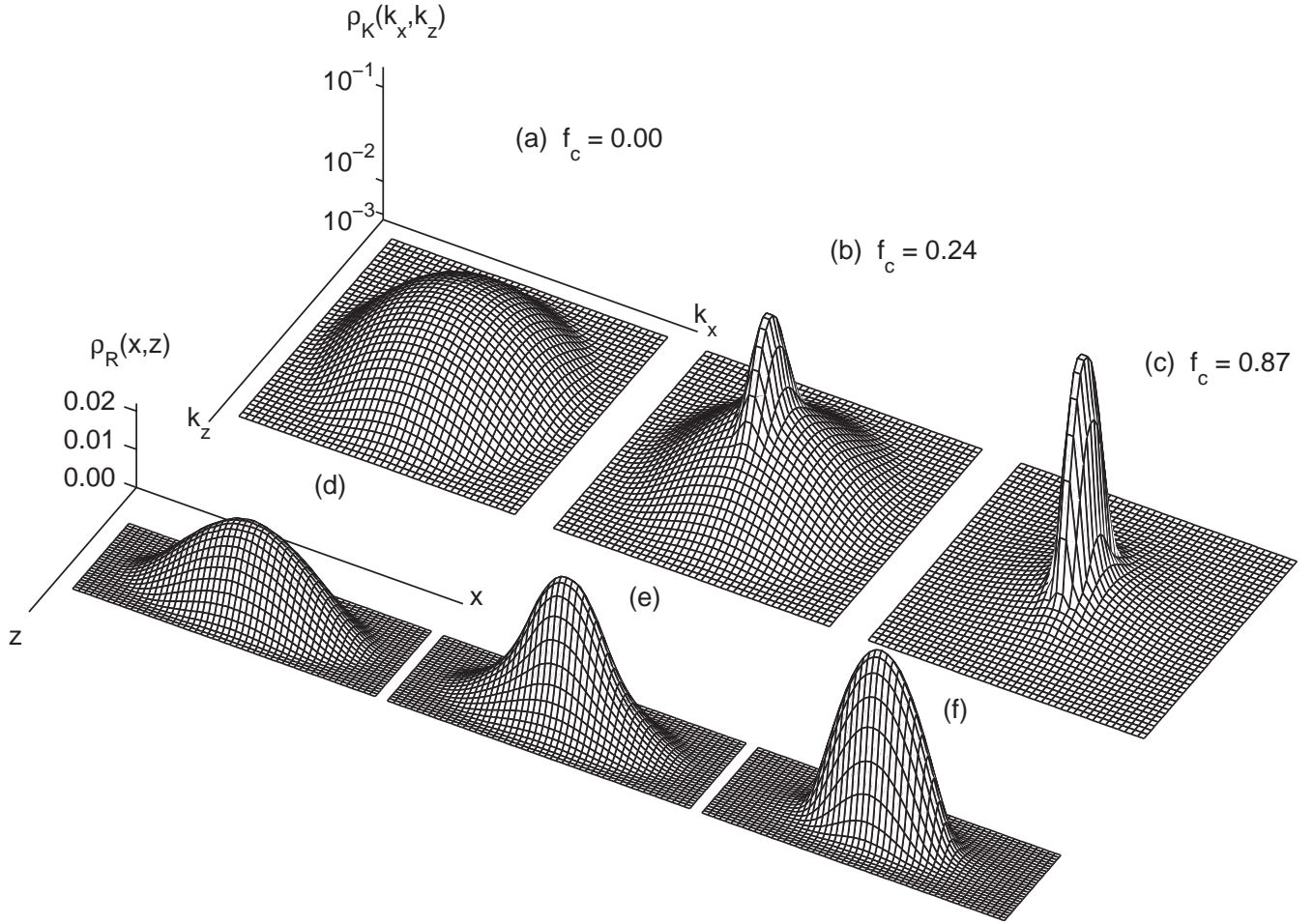


Figure 3: Time-averaged column densities in momentum (a)–(c) and position (d)–(e) space of classical field simulations with various energies. Cases: (a) and (d) $E = 24\hbar\omega_z$; (b) and (e) $E = 18\hbar\omega_z$; (c) and (f) $E = 10\hbar\omega_z$. Other simulation parameters are the same as in Fig. 1. The averaging was performed using $N_s = 1400$ samples over a evolution period of $T = 1200/\omega_z$.

spatial separation, defined as

$$g_n(\mathbf{x}) = \frac{\langle (\hat{\Psi}^\dagger(\mathbf{x}))^n (\hat{\Psi}(\mathbf{x}))^n \rangle}{\langle \hat{\Psi}^\dagger(\mathbf{x}) \hat{\Psi}(\mathbf{x}) \rangle^n}. \quad (23)$$

Once again we note that we have restricted our attention to correlation functions involving the coherent field operator. The normalized coherence functions have been calculated for the case of $n = 2$ by Dodd *et al.* [36] using Hartree-Fock-Bogoliubov theory in the Popov approximation, which should be valid for large condensate fractions. In contrast the classical field result should be applicable as long as our assumption of high mode occupancy is satisfied.

Using the ergodic averaging procedure (see section IV B) we evaluate (23) for the cases $n = 2$ and $n = 3$. The results, shown in Fig. 4, are for the case of $C = 2000$ in the pancake geometry trapping potential ($\lambda_x = \sqrt{8}$ and $\lambda_y = 1$). For reference, we note that Fig. 1 (a) corresponds to a single profile used for the results in Figs. 4 (a) and (d), and similarly Fig. 1 (b) corresponds to a single profile used for the results in Figs.

4(c) and (f). These coherence functions were evaluated by angular averaging about the symmetry axis in the $x = 0$ plane (in addition to the time-averaging), and are plotted against the radial distance from the trap center in that plane.

The coherence functions provide a useful characterisation of quantum fields. For instance $g_n = 1$ for coherent fields such as a laser, whereas $g_n = n!$ for thermal light fields. These features are clearly apparent in our results for the matter-wave field. When a condensate is present it occupies the center of the trapping potential and dominates the thermal fraction of atoms in this region. This is clearly seen in Figs. 4 (a) and (d), where for a condensate fraction of 87%, there is a shape transition from coherent behavior ($g_n = 1$) near the trap center, to thermal behavior ($g_n = n!$) at a radius of approximately $r = 5x_0$.

In Figs. 4(b) and (e) the same qualitative behavior is seen, however the smaller condensate fraction (approximately 24% for this case) causes the boundary between coherent and thermal regions to be closer to the trap center. Also, the coherence near the trap center is suppressed (i.e. slightly increased from unity), indicating that the dominant thermal fraction of

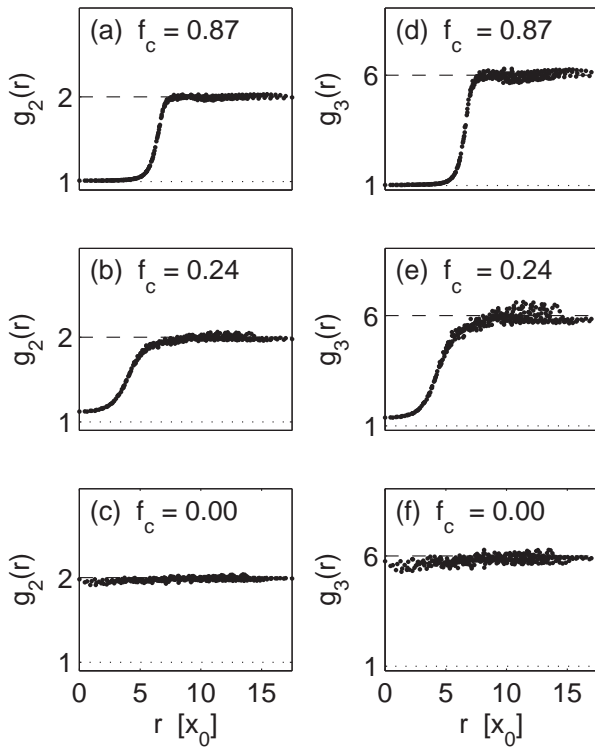


Figure 4: Normalized coherence functions $g_2(r)$ and $g_3(r)$ (see text) as a function of radial position in the $x = 0$ plane (averaged over angle about the symmetry axis), and for various condensate fractions. The simulation parameters are the same as in Fig. 1, and all results are for the case $C = 2000$. For reference the coherent value ($g_n = 1$) and thermal value ($g_n = n!$) of the coherence functions are indicated as dotted and dashed lines in the plots respectively.

the system is penetrating into the region of the condensate, or in some manner causing increased fluctuations in the condensate mode.

The results shown in Figs. 4 (c) and (f) are for sufficiently high energy that the condensate fraction is zero. For this case we find the thermal behavior ($g_n = n!$) is present everywhere in the system.

VI. APPLICATION TO NON-EQUILIBRIUM DYNAMICS

The most interesting application of the PGPE technique will be to the non-equilibrium Bose gas. In many cases this will require a quantitative description of the incoherent region, which is beyond the scope of this paper, but is the subject of on going work [15]. To give a qualitative demonstration of a non-equilibrium application, we consider a simplified simulation of evaporative cooling using the PGPE. We emphasise that this is not intended for quantitative comparison with experiment, but the calculation highlights several interesting features of the non-equilibrium dynamics, particularly in relation to the identification of the condensate.

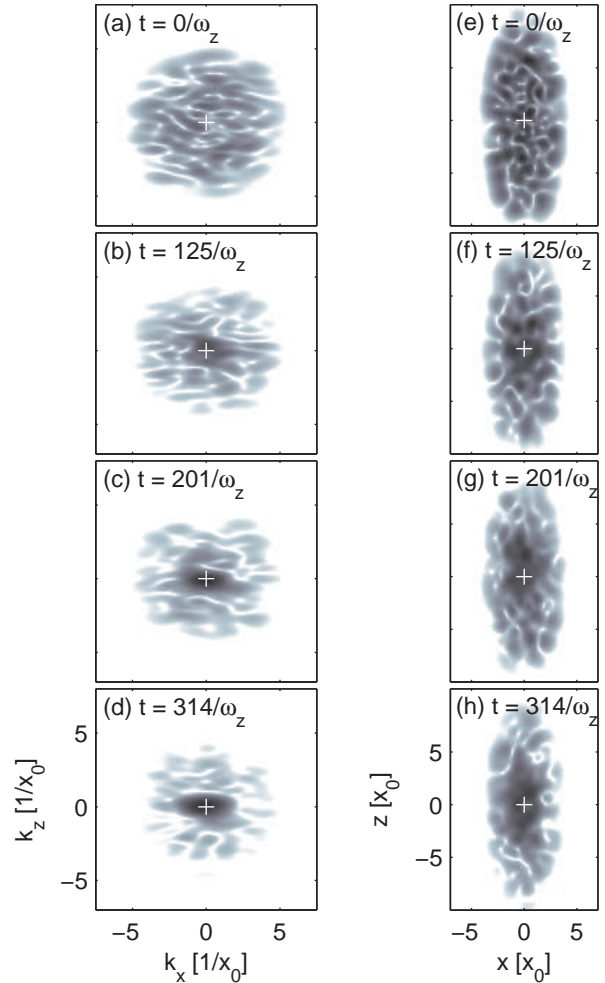


Figure 5: Evolution of an evaporatively cooled matter-wave field. (a)-(d) Momentum space density in the $k_y = 0$ plane, (e)-(h) corresponding position space density in the $y = 0$ plane. The + signs are used to indicate the zero-coordinate in the plots for reference. The initial state for the simulation is shown in Fig. 1(b), and the evaporation is applied until $t = 64\pi/\omega_z$ by setting $\Psi(\mathbf{x}) = 0$ for $|z| > 9x_0$ during the simulation. Other parameters are as in Fig. 1.

A. Evaporative cooling simulation

To perform a simulation of evaporative cooling, we begin with the classical field in an equilibrium state above the transition temperature. The cooling is implemented in a manner analogous to that used in experiments: high-energy atoms that are able to venture into regions far from the trap center are selectively removed. We do this by absorbing the portion of the classical field which extends outside the spatial region $|z| < 9x_0$ (i.e. setting it to zero at each time step of the simulation). We note that for the initial state considered [which is the same as the state shown in Fig. 1(b)] only a small fraction of the field extends into this region, and so the normalisation and energy of the classical field is lost relatively slowly during the cooling [also see Fig. 6(b)]. After 32 trap periods the cooling mechanism is turned off and the

system is allowed to evolve and rethermalize for a subsequent 20 trap periods. A summary of the classical field dynamics at instances during this simulation is shown in Fig. 5. The initial momentum and position profiles are shown in Figs. 5(a) and (e) respectively. After approximately 20 trap periods of cooling a momentum peak has developed in the distribution near $k = 0$ [see Fig. 5(b)]. During these early stages of growth the condensate undergoes strong sloshing and breathing dynamics as fierce mixing occurs between the forming condensate and other low-lying quasiparticle modes. The images in Figs. 5(c) and (g) show the field at the end of the evaporative cooling (32 trap periods). These figures show a large condensate centered about zero momentum [see Fig. 5(c)] and a relatively settled position distribution [see Fig. 5(g)]. The condensate exhibits breathing dynamics, however this is significantly quenched relative to the strong dynamics seen at earlier stages of condensate growth. The condensate at the end of the rethermalization period is shown in Figs. 5(d) and (h).

B. Time-dependent condensate fraction

>From the momentum space images of Fig. 5 it seems quite obvious when a Bose-Einstein condensate has formed. A sharp peak suddenly appears in momentum space, whereas there is no such clear signature in the real space distributions. We note that the momentum space images are on a logarithmic scale — so the peak is even more obvious using a linear scale. However, in Ref. [10] it was stated that the time-averaging inherent in the imaging process of real experiments was essential for the splitting of the system into a condensed and non-condensed fraction. Our results are in clear disagreement with this conclusion, and it is at least qualitatively apparent that condensation has occurred from a single image of the classical field.

To quantitatively investigate this observation and to examine the growth of the condensate, we first apply the Penrose-Onsager approach discussed in section V A 1 to the evaporative cooling simulation. The cooling is only carried out in one dimension, and so the dynamics proceed rather slowly. Thus it seems that we should be able to estimate the one-body density matrix at a given time by time-averaging over short periods. We calculate the condensate fraction at trap period intervals by averaging the one-body density matrix over that interval (by summing the classical field at 30 discrete instances during that interval), and diagonalizing it. The results are shown in Fig. 6(a) as the open circles. Due to the finite time over which we are able to average, the initial condensate fraction calculated is non-zero despite the initial state having zero condensate fraction. Because the system is not in equilibrium during the evaporation it is not clear that the Penrose-Onsager approach is applicable, however, the characteristic s-shaped curve we find in Fig. 6(a) is expected theoretically and has been observed experimentally (see [37] and references therein). Since the evaporative cooling mechanism is dissipative, particles and energy are lost from the system. The evolution of these quantities in the simulation are shown in Fig. 6(b). This shows that during the cooling 74% of the particles and 88% of the energy in the

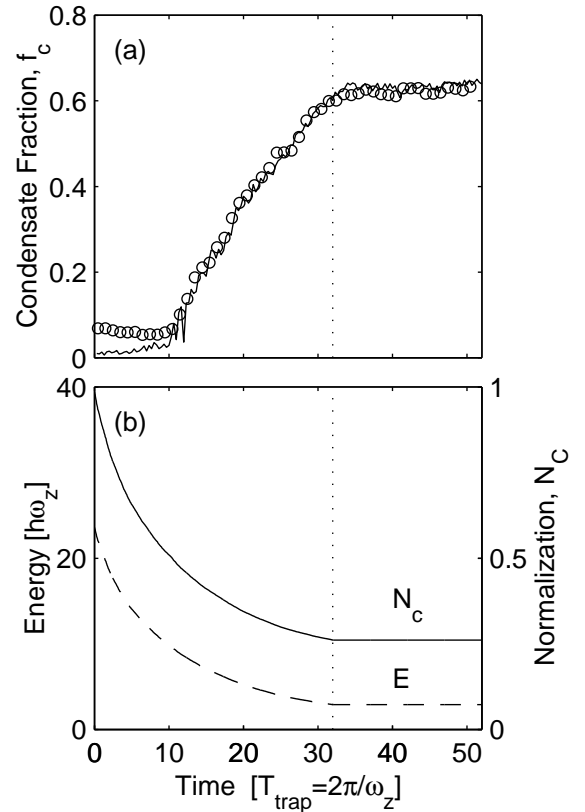


Figure 6: Growth of condensate and loss of energy and normalization during evaporative cooling process. (a) The condensate fraction of the total remaining classical field. The open circles are calculated by diagonalizing the one-body density matrix estimated by time-averaging over two trap periods, while the solid curve is calculated by fitting bimodal distributions to single-shots as described in the text. (b) The classical field energy (dashed line) and normalization (solid line) as a function of time. The point of time at which evaporation is stopped is marked by a vertical dotted line. Simulation parameters are explained in Fig. 5.

classical field is lost.

The second approach we take is to fit bimodal distributions to single-shot column densities of the classical field in momentum space. This computational method mimics the actual experimental procedure that is used for fitting condensate plus thermal cloud absorption images in the laboratory. The fitting function is the sum of two Gaussian profiles of differing widths, and three separate least-squares fits are carried out along each of the x , y , and z axes. Our fitting procedure determines the boundary of the condensate, and the condensate number is the integral of the column density in this region less the estimated density of the thermal cloud. It seems beneficial to fit column densities, as this averages over some of the fluctuations apparent in slices through planes of the classical field, in a manner reminiscent of the spatial averaging carried out in the realisation of a single trajectory in [23]. A visualisation of the results of this fitting method are displayed in Fig. 7.

The results of this second method are also shown in Fig. 6(a) as the solid curve, and the results are in remarkable agree-

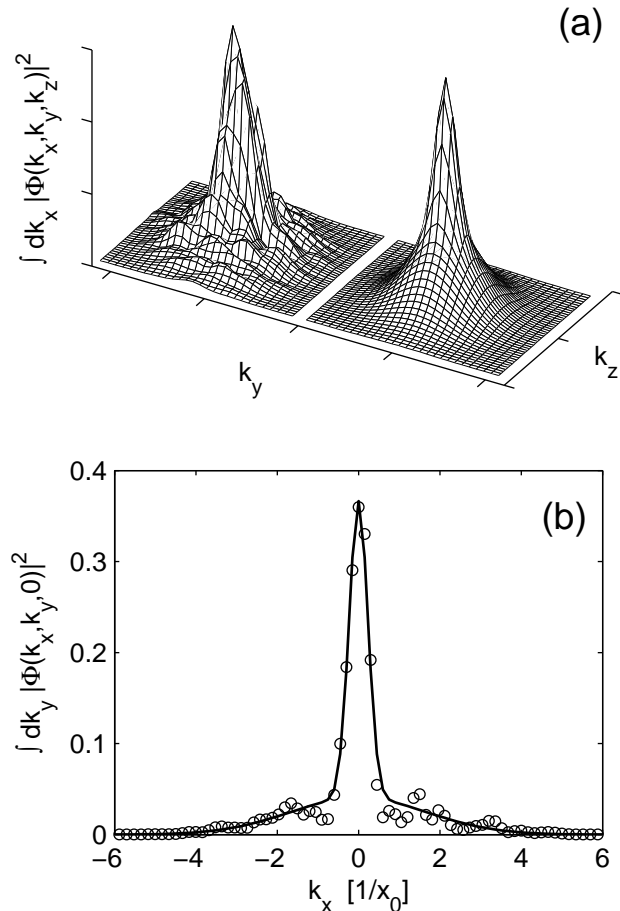


Figure 7: Example of the bimodal fitting procedure for a single-shot of a classical field with a condensate fraction of about 0.24. (a) The image on the left is the column density of the classical field, while the image on the right is the bimodal fit. (b) A slice through another column density of the same field. The open circles are the data points and the solid line is the fitted curve.

ment with the Penrose-Onsager approach. Thus it seems to us that the condensate fraction in a static harmonic trap can be estimated from a single-shot image of the classical field, without any time-averaging being necessary. In hindsight this seems obvious, as this is the standard experimental procedure and it seems to have had some success. The time-averaging that occurs due to the finite exposure time in experimental imaging is only on the order of tens of microseconds [38], which is almost instantaneous on the time-scale of the matter-wave dynamics. In particular this must be the case for non-destructive techniques such as phase-contrast imaging otherwise little information would be gained. Intuitively the Penrose-Onsager approach should require averaging over a time-scale of order a trap period. Thus it seems to us that the claim that time-averaging is necessary to identify the condensate in Ref. [10]

is incorrect. Indeed, if imaging was performed using longer duration exposures, photon recoil effects on the atoms would dominate over any averaging of the matter wave dynamics (e.g. see Sec. 3.5.2 of Ref. [39]). A question of interest is how the methods we have used here would perform in strongly non-equilibrium situations, however we leave this investigation for future work.

As a final remark, we again wish to emphasise that the simulation example neglects physical processes which would be important in a quantitative model of an evaporative cooling experiment. This arises through our ignorance of the incoherent region which would be responsible for the significant transfer of particles and energy into the coherent region. However, this model does help to illustrate the rather complex dynamics that occur in the coherent region as it responds to the selective removal of high energy components. The PGPE method models the complete non-perturbative dynamics of the low-lying modes and is naturally suited to considering non-equilibrium situations such as evaporative cooling.

VII. CONCLUSIONS

In this paper we have presented an efficient numerical scheme for implementing the Projected Gross-Pitaevskii equation formalism in three-dimensional harmonic traps without any axis of symmetry. The main feature of this scheme is that it implements a consistent energy cutoff in the harmonic oscillator basis and is suitable to efficient and accurate numerical simulation on modern computer workstations. As an application of the method we have used it to simulate a finite temperature Bose gas in an anisotropic harmonic trap both above and below the critical temperature. Using the ergodic hypothesis we have obtained equilibrium quantities such as the condensate fraction and the temperature for these simulations, and have calculated the second- and third-order normalized coherence functions. As a non-equilibrium application we have used the PGPE to simulate the growth of a condensate from an evaporatively cooled thermal cloud. We have managed to identify the condensate fraction in this calculation from both the diagonalization of the time-averaged density matrix, as well as single-shot column densities in momentum space of the classical field.

Acknowledgements

PBB would like to thank Charles W. Clark of NIST for support during the initial stages of this work, and the Otago Lasers and Applications Research Theme for the computational resources essential to the calculations reported. MJJ acknowledges the support of the ARC Centre of Excellence for Quantum-Atom Optics.

-
- [1] B. V. Svistunov and G. V. Shlyapnikov, *J. Mosc. Phys. Soc.* **1**, 373 (1991).
- [2] Y. Kagan, B. V. Svistunov, and G. V. Shlyapnikov, *Zh. Éksp. Teor. Fiz.* **101**, 528 (1992), [*JETP* **75**, 387 (1992)].
- [3] Y. Kagan and B. V. Svistunov, *Zh. Éksp. Teor. Fiz.* **105**, 353 (1994), [*JETP* **75**, 387 (1992)].
- [4] Y. Kagan and B. V. Svistunov, *Phys. Rev. Lett.* **79**, 3331 (1997).
- [5] R. J. Marshall, G. H. New, K. Burnett, and S. Choi, *Phys. Rev. A* **66**, 2085 (1999).
- [6] M. J. Davis, S. A. Morgan, and K. Burnett, *Phys. Rev. Lett.* **87**, 160402 (2001).
- [7] M. J. Davis, S. A. Morgan, and K. Burnett, *Phys. Rev. A* **66**, 053618 (2002).
- [8] M. J. Davis and S. A. Morgan, *Phys. Rev. A* **68**, 053615 (2003).
- [9] K. Góral, M. Gajda, and Rzążewski, *Opt. Express* **8**, 92 (2001).
- [10] K. Góral, M. Gajda, and K. Rzążewski, *Phys. Rev. A* **66**, 051602(R) (2002).
- [11] H. Schmidt, K. Góral, F. Floegel, M. Gajda, and K. Rzążewski, *J. Opt. B* **5**, 96 (2003).
- [12] M. Brewczyk, P. Borowski, M. Gajda, and K. Rzążewski, *J. Phys. B* **37**, 2725 (2004).
- [13] M. J. Davis, R. J. Ballagh, and K. Burnett, *J. Phys. B* **34**, 4487 (2001).
- [14] C. W. Gardiner, J. R. Anglin, and T. I. A. Fudge, *J Phys. B* **35**, 1555 (2002).
- [15] C. W. Gardiner and M. J. Davis, *J Phys. B* **36**, 4731 (2003).
- [16] M. J. Steel, M. K. Olsen, L. I. Plimak, P. D. Drummond, S. M. Tan, M. J. Collett, and D. F. Walls, *Phys. Rev. A* **58**, 4824 (1998).
- [17] A. Sinatra, Y. Castin, and C. Lobo, *J. Mod. Opt.* **47**, 2629 (2000).
- [18] A. Sinatra, C. Lobo, and Y. Castin, *Phys. Rev. Lett.* **87**, 210404 (2001).
- [19] A. Sinatra, C. Lobo, and Y. Castin, *J. Phys. B* **35**, 3599 (2002).
- [20] A. Polkovnikov, *Phys. Rev. A* **68**, 053604 (2003).
- [21] A. Polkovnikov and D.-W. Wang, *Phys. Rev. Lett.* **93**, 070401 (2004).
- [22] C. Lobo, A. Sinatra, and Y. Castin, *Phys. Rev. Lett.* **92**, 020403 (2004).
- [23] A. A. Norrie, R. J. Ballagh, and C. W. Gardiner, *cond-mat/0403378* (2004).
- [24] L. Isella and J. Ruostekoski, *cond-mat/0409475* (2004).
- [25] C. M. Dion and E. Cancès, *Phys. Rev. E* **67**, 046706 (2003).
- [26] M. J. Davis, in preparation (2004).
- [27] F. Dalfovo, S. Giorgini, L. Pitaevskii, and S. Stringari, *Rev. Mod. Phys.* **71**, 463 (1999).
- [28] A. S. Bradley and P. B. Blakie and C. W. Gardiner, in preparation (2004).
- [29] H. H. Rugh, *Phys. Rev. Lett.* **78**, 772 (1997).
- [30] O. Penrose and L. Onsager, *Phys. Rev.* **104**, 576 (1956).
- [31] S. Giorgini, L. P. Pitaevskii, and S. Stringari, *Phys. Rev. A* **54**, R4633 (1996).
- [32] F. Gerbier, J. H. Thywissen, S. Richard, M. Hugbart, P. Bouyer, and A. Aspect, *Phys. Rev. Lett.* **92**, 030405 (2004).
- [33] M. J. Davis and P. B. Blakie, in preparation (2004).
- [34] M. H. Anderson, J. R. Ensher, M. R. Matthews, C. E. Wieman, and E. A. Cornell, *Science* **269**, 198 (1995).
- [35] J. Stenger, S. Inouye, A. P. Chikkatur, D. M. Stamper-Kurn, D. E. Pritchard, and W. Ketterle, *Phys. Rev. Lett.* **82**, 4569 (1999).
- [36] R. Dodd, C. W. Clark, M. Edwards, and K. Burnett, *Opt. Express* **1**, 284 (1997).
- [37] M. Köhl, M. J. Davis, C. W. Gardiner, T. W. Hänsch, and T. Esslinger, *Phys. Rev. Lett.* **88**, 080402 (2002).
- [38] M. Barrett, private communication.
- [39] W. Ketterle, D. S. Durfee, and D. M. Stamper-Kurn, in *Proceedings of the International School of Physics - Enrico Fermi*, edited by M. Inguscio, S. Stringari, and C. E. Wieman (IOS Press, 1999), p. 67.